

Received October 11, 2020, accepted October 30, 2020, date of publication November 6, 2020, date of current version November 18, 2020.

Digital Object Identifier 10.1109/ACCESS.2020.3036380

Deep DIH: Single-Shot Digital In-Line Holography Reconstruction by Deep Learning

HUAYU LI¹, XIWEN CHEN¹, (Student Member, IEEE), ZAOYI CHI¹,
CHRISTOPHER MANN², AND ABOLFAZL RAZI¹, (Senior Member, IEEE)

¹School of Informatics, Computing, and Cyber Systems, Northern Arizona University, Flagstaff, AZ 86011, USA

²Department of Materials Science, Northern Arizona University, Flagstaff, AZ 86011, USA

Corresponding author: Abolfazl Razi (abolfazl.razi@nau.edu)

This work was supported in part by the Arizona Board of Regents under Grant 1003329.

ABSTRACT Digital in-line holography (DIH) is broadly used to reconstruct 3D shapes of microscopic objects from their 2D holograms. One of the technical challenges in the reconstruction stage is eliminating the twin image originating from the phase-conjugate wavefront. The twin image removal is typically formulated as a non-linear inverse problem since the scattering process involved in generating the hologram is irreversible. Conventional phase recovery methods rely on multiple holographic imaging at different distances from the object plane along with iterative algorithms. Recently, end-to-end deep learning (DL) methods are utilized to reconstruct the object wavefront (as a surrogate for the 3D structure of the object) directly from the single-shot in-line digital hologram. However, massive data pairs are required to train the utilize DL model for an acceptable reconstruction precision. In contrast to typical image processing problems, well-curated datasets for in-line digital holography do not exist. The trained models are also highly influenced by the objects' morphological properties, hence can vary from one application to another. Therefore, data collection can be prohibitively laborious and time-consuming, as a critical drawback of using DL methods for DH. In this article, we propose a novel DL method that takes advantages of the main characteristic of auto-encoders for blind single-shot hologram reconstruction solely based on the captured sample and without the need for a large dataset of samples with available ground truth to train the model. The simulation results demonstrate the superior performance of the proposed method compared to the state-of-the-art methods used for single-shot hologram reconstruction.

INDEX TERMS Digital holography, phase reconstruction, twin image removal, deep learning, digital microscopy.


I. INTRODUCTION

Digital holography (DH) is a powerful imaging technique used to reconstruct the three-dimensional (3D) surface of an object from its two dimensional (2D) image captured by a visual sensor. It is considered a digital microscopy suitable for micro-scaled and nano-scaled objects which is used in a wide range of applications including chemistry [1], biomedical microscopy [2], nano-material fabrication [3], [4], and nano-security [5].

Digital holography can be used in different modalities, including that of *in-line digital holography*, i.e. transmission imaging of transparent objects [6]. The sample modulates the

wavefront phase of the emitted beam. The 3D structure of the object can be easily reconstructed from the recovered phase information, as shown in Fig.1.

Regardless of the object type, there are two main implementation approaches for digital holography, *off-axis holography* [7], and *in-line holography* [8]. In off-axis holography, the laser beam is split into two waves, the reference wave denoted by R and object wave denoted by O , where only the latter passes through the object. The two waves are combined with a small relative incidence angle θ at the exit of the interferometer to create the hologram intensity as $I_H(x, y) = |R^2 + |O|^2 + R^*O + RO^*$, where X^* denotes the complex conjugate of X . The relative angle causes the real images and *twin images* to form separable locations in Fourier space. This spatial separation facilitates simple phase recovery through

The associate editor coordinating the review of this manuscript and approving it for publication was Senthil Kumar .

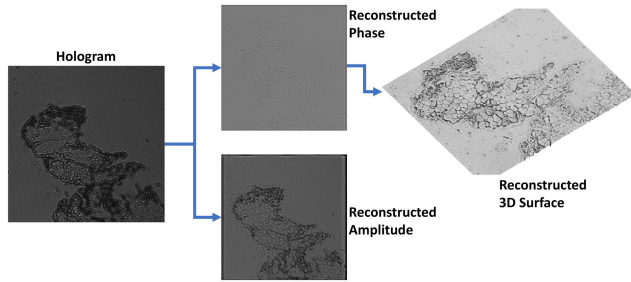


FIGURE 1. The amplitude and phase of the wavefront can be extracted from the recorded hologram using numerical reconstruction methods. The phase information represents the surface depth or the thickness of the object, which can be used to reconstruct the object’s 3D view. This figure shows how digital holography records the 3D information of an object into a 2D form.

filtering in the Fourier domain. On the other hand, the off-axis technique requires additional experimental effort, and because of the spatial filtering in the Fourier Domain there may be appreciable resolution loss. In comparison, in-line holography allows for high resolution phase recovery through simple, inexpensive apparatus without the need to use any magnifying components such as objective lenses. Only a single beam path is required for the setup. In addition, numerical refocusing through diffraction algorithms based on the *Fresnel-Kirchhoff* such as the *Angular Spectrum* or *Fresnel approximation* eliminate the need for actuating mechanical devices for focusing.

One significant disadvantage of in-line holography is that it has to contend with the twin image problem, which is the result of the loss of phase information in the final refocused image [9]. The recorded hologram image contains both the real and virtual image superimposed upon each other along with the DC (zeroth order term). These terms are not separable in the Fourier Domain. To uniquely recover one of the holographic terms containing the phase information, phase-retrieval iterative algorithms may be applied [10]–[14]. If the phase is recovered accurately, the twin image will be highly suppressed [15], [16]. From the recovered phase information, the 3D surface profile of the sample may be easily obtained if the refractive index is known.

The simplicity of sample preparation without the need for sectioning, as well as staining, and its high-speed imaging capabilities make the in-line holography well suited for the investigation of biological specimens [2].

II. PROBLEM STATEMENT

To further explore the physical model behind the concept of *twin image removal*, we investigate the process of DIH, as shown in Fig.3. Suppose that we have an object field $\rho(x, y)$ and the propagation transfer function $h(x, y)$, then the scattered wave $O(x, y)$ can be described as [17]:

$$O(x, y) = \iint_{x_i, y_i \in \Sigma} \rho(x_i, y_i) h(x - x_i, y - y_i) dx_i dy_i \quad (1)$$

where Σ represents an aperture window. The transmittance function $h(x, y)$ depends on the light wavelength λ and the

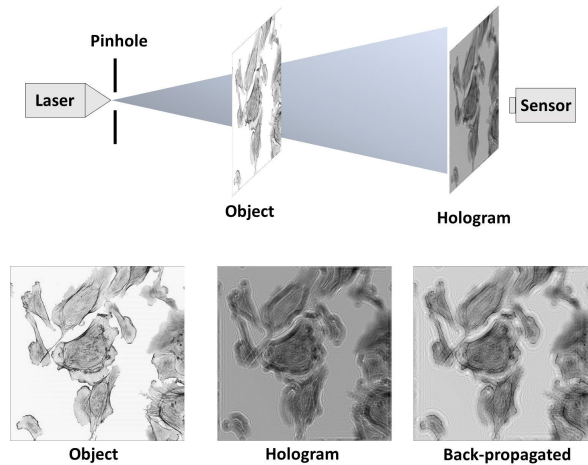


FIGURE 2. The illustration of the basic inline holography setup and the twin-image issue: the scattered object wave interferes with the unscattered reference wave in the inline holography and creates the twin image. This effect is shown in the recorded hologram (bottom-middle) and the back propagated image (bottom-right).

propagation distance z between the image plane and the hologram. The transfer function in the frequency domain is:

$$H(f_x, f_y) = \exp(ikz\sqrt{1 - (\lambda f_x)^2 - (\lambda f_y)^2}) \quad (2)$$

where $k = 2\pi/\lambda$ is the wave number. In addition to the diffracted wave $O(x, y)$, there exists a non-scattered reference wave $R(x, y)$. The Hologram $I_H(x, y)$ records the intensity of the mixed waves captured by the light sensors and can be expressed as:

$$I_H = |O + R|^2 = O^*R + OR^* + |O|^2 + |R|^2 = U(x, y) + U^*(x, y) + |O|^2 + |R|^2 \quad (3)$$

where we define $U(x, y) = O^*R$ for notation convenience. The captured hologram includes the object field $O(x, y)$ and its conjugation $O(x, y)$, respectively, representing the virtual and real images [6]. This phenomenon leads to the formation of the twin image, an issue to be dealt with in the reconstruction phase. As one focuses on one of the holographic terms, the out of focus conjugate smears the reconstructed image.

Note that the reference field ($|R|^2$) can be assumed one without the loss of generality and can be removed from the hologram. Also, the term $|O|^2$ can be regarded as the noise term $n(x, y)$. Therefore, reconstructing the object field boils down to removing the twin image [17], which has been the center of attention in many prior works [2], [11], [18], [19]. If we define transformation $T : \rho(x, y) \mapsto U(x, y)$, the image reconstruction can be recast as the following standard inverse problem:

$$I_H(x, y) = 2\text{Re}[T(\rho(x, y))] + n(x, y). \quad (4)$$

Both $U(x, y)$ and its conjugation $U^*(x, y)$ are interchangeably consistent with the solution of Eq (4); therefore it can be regarded as an under-determined problem. Also, standard

inverse problems can not be utilized to solve Eq (4), since it includes the non-linear transformation.

There exist several means for solving the twin image problem. Recording a collection of holograms at different propagation distances and reconstructing the object field by the *transport of intensity* (TIE) method has yielded promising results [20], [21]. Most conventional phase retrieval methods use the following TIE imaging equation to recover the phase term $\phi(x, y)$ [19], [22], [23]:

$$\frac{\partial I(x, y)}{\partial z} = -\frac{\lambda}{2\pi} \nabla(I(x, y) \nabla \phi(x, y)), \quad (5)$$

where $I(x, y)$ is the hologram intensity, λ is the wavelength, and ∇ is the gradient operator in the lateral dimensions (x, y) [19]. When the intensity is constant (or normalized), the following simplified equations can be used to recover $\phi(x, y)$ [18], [19], [24]:

$$\frac{2\pi}{\lambda I} \frac{\partial I(x, y)}{\partial z} = \nabla^2 \phi(x, y). \quad (6)$$

Several extensions to the TIE method are proposed in the literature to extend it for different applications including volume holography [25], and holographic x-ray imaging [26]. One technical difficulty in solving Eqs (5) and (6) is the need for multiple imaging at fine-tuned distances from the focal plane (i.e., $\Delta z, 2\Delta z, \dots$) to precisely quantify the gradient term $\partial I(x, y)/\partial z$ using least square method [27], hybrid linearization method [28], [29], and iterative methods [18].

Therefore, developing methods that can recover phase information from only one recording has obvious practical advantages. *Phase retrieval* (PR) is one of the most commonly used numerical approaches which perform double-side constraint iteration with a specific support region [30]. Mathematically, the in-line hologram provides an undesirable component that can result in the loss of phase information. PR permits the separation of real-object distribution from the twin-image interference. Gerchberg-Saxton (GS) algorithm [11], [13], [14], [31] and hybrid input-output (HIO) algorithm [32], [33] perform iterative phase retrieval with the following steps for object wave R , reference wave O , and initial guess of the object phase Ω_0 :

- **Step 1:** Let $|R + O_n|e^{i\Omega_n}$ be a trial scattering density in the n^{th} iteration cycle, and ρ_n is the back-propagated results of $|R + O_n|e^{i\Omega_n}$.
- **Step 2:** Impose constraints to ρ^n in the support region, and obtain ρ^{n+1} .
- **Step 3:** Forward-propagate ρ^{n+1} to obtain $|R + O_{n+1}|$.
- **Step 4:** Update the phase $\Omega_{n+1} = \text{Angle}(R + O_{n+1})$.

The inconsistency region γ is the area where the reconstructed image in the current iteration does not satisfy the object constraint, or a region we are not interested in performing the phase retrieval. In step 2 of the GS algorithm, we impose the constraints as follows

$$\rho^{n+1} = \begin{cases} 0 & \rho^n \in \gamma; \\ \rho^n & \rho^n \notin \gamma; \end{cases} \quad (7)$$

while the HIO algorithm deploys a relaxing factors β to reduce the probability of stagnation that contains feedback information concerning previous iterations as:

$$\rho^{n+1} = \begin{cases} \rho^n - \beta \rho^n & \rho^n \in \gamma; \\ \rho^n & \rho^n \notin \gamma. \end{cases} \quad (8)$$

Although PR shows excellent performance on the object reconstruction. Due to the double-side constraint iteration with a specific support region, the reconstruction area is under a severe limitation, that the reconstruction performs bad when the desired object has lot of textural and structural details.

Recently, deep learning-based (DL-based) methods have been widely used in phase and amplitude reconstruction problems, such as deep MRI reconstruction [34]–[37], as well as end-to-end digital hologram reconstruction [38]–[40] with proven Superior efficiency. This is due to the power of convolutional neural networks (CNNs) that are widely used as a universal approximator for solving inverse problems in the field of computer vision. The general approach is training a CNN on training data pairs (holograms, and twin image-free phase and amplitude), then using the well-trained CNNs to reconstruct the twin image-free results. For instance, [34] offers a DL method based on residual complex convolutional networks to reconstruct multi-channel MRI images. This method is similar to our method in a sense that it recovers the real and imaginary part of complex-valued images. However, it is not directly applicable to digital holography, where the real and imaginary parts of the hologram follow the aforementioned specific wave equations (1-3), and noting the fact that only the intensity of the holographic images is available in our method.

DL methods rely on large datasets in the training phase. In most DL-based image processing tasks, massive training datasets are easily accessible. However, obtaining datasets for digital holography, especially when applied to bio-samples, can be costly since collecting bio samples, capturing holograms, and generating the corresponding ground truth are pretty difficult and laborious. Meanwhile, CNNs are regarded as black boxes when the training and inferring steps are invisible and unexplainable. This means when using a well trained CNN to reconstruct the hologram, it is impossible to deal with the upcoming problems if the reconstruction is not correct.

In [17], an algorithm based on compressive sensing (CS) is proposed to reconstruct a twin image-free hologram. The CS method is able to remove the twin image from a single-shot hologram and does not require a training dataset. As a physics-driven method, the CS method exploits the sparsity difference between the reconstructed object and the twin image by filtering out the diffused conjugated signal by imposing sparsity constraints on the object plane. The total variation (TV) norm is suitable for removing the twin image since the in-focus object has sharp edges, while the out-of-focus twin image is diffuse. A two-step iterative shrinkage/thresholding (TwIST) algorithm is used in [17] to address

the twin image removal problem. their approach is minimizing an objective function formed from two terms, the mean squared error (MSE) and TV norm, namely

$$\hat{\rho} = \arg \min_{\rho} \left\{ \frac{1}{2} \|H - T(\rho)\|_2^2 + \tau \|\rho\|_{tv} \right\}, \quad (9)$$

where τ is the relative weight between the TV norm $\|\rho\|_{tv} = \sum_i \sqrt{|\Delta_i^x \rho|^2 + |\Delta_i^y \rho|^2}$ and the MSE term. The Δ_i^x and Δ_i^y refer to the horizontal and vertical first-order gradients, respectively, and ρ is the object field as before. The reconstruction with denser edges suffers from a more out-of-focus twin image effect [41] and has a larger TV norm. The CS method has been proven more effective than the conventional PR algorithms [30], [42], [43] in terms of removing the twin image from the recorded holograms. However, this method suffers from a couple of problems. Accurate tuning of τ that makes a trade-off between the TV norm and the MSE terms for optimal twin image removal is not straightforward. Note that the large values of τ can result in a blurry reconstructed image, while the small values of τ undermine the efficiency of twin image removal. Also, imposing severe sparsity constraints on the image restoration can lead to edge distortion.

The above-mentioned facts reveal the need for developing an efficient reconstruction algorithm that is (i) suitable for one-shot imaging, and (ii) does not require a large training dataset. In this article, a novel DL-based algorithm is proposed based on fitting an auto-encoder to the possible solutions of physics-driven holography equations. Like other uses of autoencoders, no training dataset is required, as a key advantage for our method. This method simultaneously performs noise reduction and twin image removal by a well-defined objective function. In the presented method, we do not suppress or remove the twin image in the reconstruction. Instead, we directly adjust the weights of the utilized DL architecture to search for the intensity and phase of the target 3D object most consistent with the captured hologram. We show that the neural network equipped with convolutional layers naturally tends to produce a more precise result. Experimental results prove the feasibility and the superior performance of the proposed method over the existing CS methods.

III. METHODS

A. DEEP LEARNING SCHEME

For the reconstruction, we use a deep network with encoder-decoder¹ architecture, the so-called *auto-encoder* which maps a high dimensional input x into a low dimensional latent code $z = f_{encode}(x)$ and reconstructs a high dimensional output $\hat{x} = f_{decode}(z)$ from the latent code. When used for supervised image restoration, the objective function is designed to penalize the error between the output \hat{x} and the ground truth y . For the unsupervised denoising

¹Note that the source code is available online at <https://github.com/XiwenChen-NAU/DeepDIH> and more information can be found at <https://www.cfnns.nau.edu/ar2843/Dendrite/dendrite.html>.

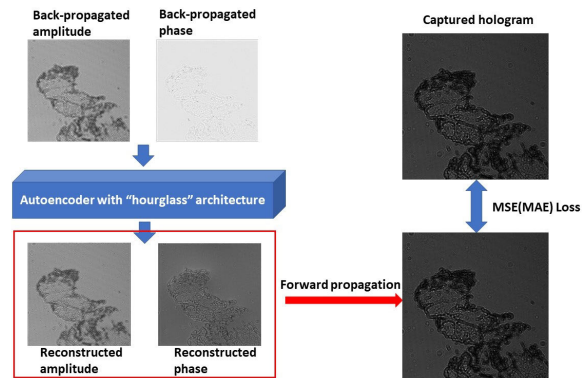


FIGURE 3. The overall block diagram of the proposed learning procedure. After feeding a fixed input (as the initial guess) into the network, the network reconstructs the image. The reconstructed result is propagated to the hologram plane by the transmission, depending on the optical parameters. The network updates its weights by minimizing the pixel-wise error between the forward-propagated result and the captured hologram.

application, the error between the input and the output is minimized to achieve the smoothest output consistent with the input. In [44], an unsupervised blind image restoration method called deep image prior (DIP) is implemented that fits a randomly initialized CNN to a single corrupted image. This method is able to recover the clean image since the CNNs could naturally learn the uncorrupted and realistic parts when the networks are underfitting to the noisy and corrupted term. Inspired by DIP, we consider using a similar approach here to remove the twin image from the reconstructed object plane. But another problem arises here due to the high coupling between the virtual and real object planes in both spatial and frequency domains. Therefore, the CNN will generate an output contaminated with the twin image, although it is clear from the noise. As mentioned in [17], the twin image term is denser than the object term. Here, we investigate a novel learning procedure using the physical model in the training process's objective function, as shown in Fig. 3. Consider an autoencoder with randomly initialized weights w to be trained to minimize a properly defined objective function, the reconstructed output ρ can be expressed as $\rho = f(x, w)$, where x is a fixed input. The objective function can be formulated as:

$$w = \arg \min_w \|H - T(f(H, w))\|_2^2, \quad (10)$$

where we want to propagate the reconstructed object wave to the hologram plane with transmission T and minimize the error between the captured hologram and the forward-propagated result. When minimizing the objective function, the network indeed searches for the optimal results by tuning the model parameters within the parameter space. Through the experiments we conduct, which will be shown later in this article in Section. IV-A, the network tends first to generate the primary instance, which is the rough shape estimate of the reconstructed object. Then the network gradually recovers the details of the object from coarse to fine. This approach, when

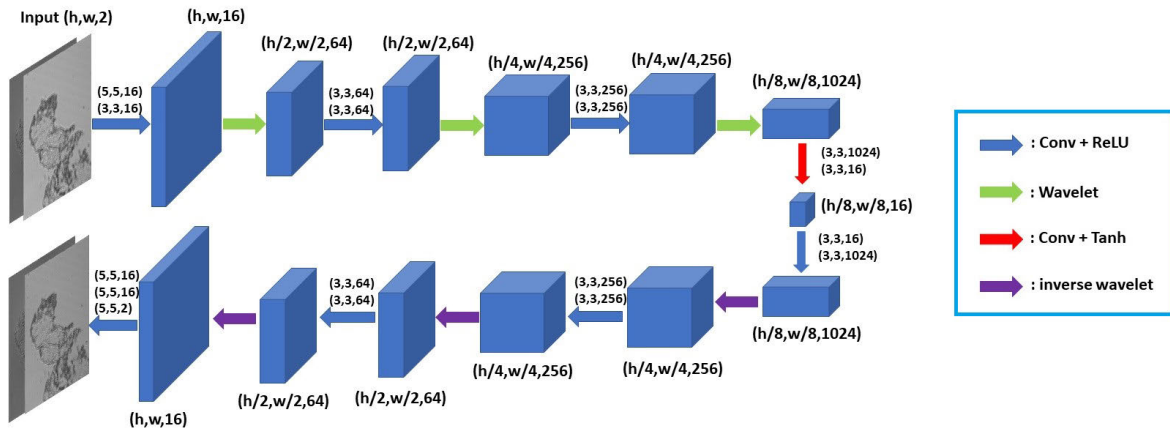


FIGURE 4. Deep convolutional autoencoder with “hourglass” architecture. Batch normalization is deployed after each convolution layer except for the last three layers to stabilize the training steps. The hyper-parameters (e.g., the kernel size and feature channels for each layer) is shown. The network is fully convolutional that enables us to feed inputs with different sizes.

applied to similar image recovery tasks such as denoising and super-resolution, may overfit the degraded term in the corrupted image. However, in the case of hologram reconstruction, both the twin image and the clean object could be the solution of the non-linear inverse problem. After generating the main body of the object, the network continues to generate the fine details of the clean object instead of the twin image.

B. IMPLEMENTATION OF AUTO-ENCODER

We first built an Auto-encoder with a “Hourglass” architecture. The encoder $f_e(\bar{\rho})$ maps the fixed network input into lower-dimensional space (encoding), and the decoder $f_d(f_e(\bar{\rho}))$ reconstructs the object from its representation by the latent variables (decoding). Batch Normalization [45] and ReLU activation [46] is used after most layers for accelerating the model convergence. The network architecture which includes the hyper-parameters, the kernel size, and channels of each layer is shown in Fig 4. *Wavelet transform* and its inverse transform are used to realize downsampling (encoding) and upsampling (decoding) which replace the pooling, strided convolution, or interpolation. According to a previous work [47], using a wavelet transform could impose sparsity on the reconstruction plane and result in more precise reconstruction with lower distortion, and our experiments verify this characteristic. Here, we use 2D Haar wavelet and its inverse transform in the encoding and decoding stages. The 2D Haar wavelet decomposes the input image or the feature map into four sub-bands by four convolutional filters (one low pass filter f_{LL} , and three high pass filters f_{LH} , f_{HL} , and f_{HH}). The four filters are defined as: $f_{LL} = \begin{bmatrix} +1 & +1 \\ +1 & +1 \end{bmatrix}$, $f_{LH} = \begin{bmatrix} -1 & -1 \\ +1 & +1 \end{bmatrix}$, $f_{HL} = \begin{bmatrix} -1 & +1 \\ -1 & +1 \end{bmatrix}$, and $f_{HH} = \begin{bmatrix} +1 & -1 \\ -1 & +1 \end{bmatrix}$. The four sub-bands are obtained by convolving the input x with the four filters, i.e. $x_{LL} = (f_{LL} \otimes x)$, $x_{LH} = (f_{LH} \otimes x)$, $x_{HL} = (f_{HL} \otimes x)$, and $x_{HH} = (f_{HH} \otimes x)$, where \otimes is the convolution operator. The inverse transform of the Haar wavelet in the (x, y) position

can be written as:

$$\begin{aligned}
 x(2i-1, 2j-1) &= \frac{1}{4}(x_{LL}(i, j) - x_{LH}(i, j) - x_{HL}(i, j) \\
 &\quad + x_{HH}(i, j)), \\
 x(2i-1, 2j) &= \frac{1}{4}(x_{LL}(i, j) - x_{LH}(i, j) + x_{HL}(i, j) \\
 &\quad - x_{HH}(i, j)), \\
 x(2i, 2j-1) &= \frac{1}{4}(x_{LL}(i, j) + x_{LH}(i, j) - x_{HL}(i, j) \\
 &\quad - x_{HH}(i, j)), \\
 x(2i, 2j) &= \frac{1}{4}(x_{LL}(i, j) + x_{LH}(i, j) + x_{HL}(i, j) \\
 &\quad + x_{HH}(i, j)). \tag{11}
 \end{aligned}$$

It is notable that during our experiment, we found out that if skip-connection (i.e. connecting lower level features to higher level layers by skipping the intermediate layers) is used in the CNN architecture similar to the U-Net [48] architecture, the network will directly project the input to the output instead of learning a clear reconstruction. This might be desirable in regular image restoration, but not for the phase retrieval process. The same concept applies when the number of channels after encoding is significantly high. To avoid this issue, we compress the feature channels at the output of the encoder from 1024 into 16 channels shown by a red arrow in Fig. 4.

IV. EXPERIMENTS

We implement our model using the PyTorch Framework [49] in a GPU workstation with an NVIDIA Quadro RTX5000 graphics card. Adam optimizer [50] is adopted with a fixed learning rate of 0.0005 for simulation-based experiments and 0.01 for optical experiments. We train the network with an angular spectrum propagation (ASP) back-propagation reconstruction as input for 1500 to 3500 iterations for simulated holograms, and 2500 to 5000 iterations for real-world holograms, respectively. There exists no public dataset for

in-line digital holography. Therefore, we used the cell image from [17], the USAF resolution chart commonly used in in-line digital holography research works, a handcrafted π and circle image, and other bio-images randomly chosen from the internet for our simulation experiments. We also use our own samples, available in Dr. Mann's research laboratory to test the performance of our method for real-world applications under more realistic conditions such as imaging artifacts.

A. SIMULATION RESULTS

In this section, several experiments are conducted for comparing our method against the CS-based method [17] using different simulated holograms which verify the superiority of proposed method over the state-of-the-art CS-based algorithm in terms of twin-image removal and precise phase reconstruction. We compare our method against the CS method, since it has shown a superior performance with respect to the majority of numerical phase retrieval methods.

We set the relative weight of TV norm between 0.01 to 0.1, and trained the algorithm between 150 to 350 iterations, for different holograms. The following Tree metrics are used to evaluate the reconstruction quality. The mean squared error (MSE) that measures the average of the squares of the pixel-wise errors between the ground truth image and reconstructed image defined as

$$MSE(x, y) = \frac{1}{MN} \sqrt{\sum_{i,j}^{N,M} (x_{i,j} - y_{i,j})^2}; \quad (12)$$

for images x and y of size $M \times N$, where $x_{i,j}$ is the pixel of x at position (i, j) .

The peak signal-to-noise ratio (PSNR) is an engineering term for the ratio between the maximum power of a signal and the power of the corrupting noise that affects the fidelity of its representation. PSNR is most easily defined via the MSE as follows

$$PSNR(x, y) = \frac{\max_{(i,j)} \{x_{ij}^2\}}{MSE(x, y)}. \quad (13)$$

The structural similarity index (SSIM) [51] is a perceptual metric that quantifies the image quality degradation caused by processing such as data compression or transmission errors. The SSIM has been proven to be more consistent with the human visual system compared to PSNR and MSE. The SSIM quantifies the changes in the structural information by inspecting the relationship among the image contrast, luminance, and structural components. The SSIM between two images is given by:

$$SSIM(I_1, I_2) = \frac{(2\mu_{I_1}\mu_{I_2} + C_1)(2\sigma_{I_1I_2} + C_2)}{(\mu_{I_1}^2 + \mu_{I_2}^2 + C_1)(\sigma_{I_1}^2 + \sigma_{I_2}^2 + C_2)} \quad (14)$$

where μ_{I_1} , μ_{I_2} , σ_{I_1} , σ_{I_2} , and $\sigma_{I_1I_2}$ are the local means, standard deviations, and cross-covariance for images I_1 and I_2 . C_1 and C_2 are two variables to stabilize the division with a weak denominator.

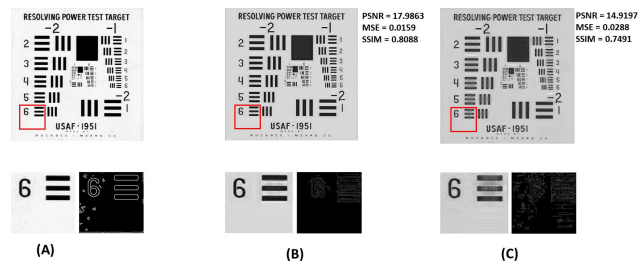


FIGURE 5. The USAF resolution chart's reconstruction intensity, the enlarged area from the reconstruction, and the edge matrix obtained by the Canny edge detector. (A) ground truth; (B) the proposed method; (C) CS method [17]. Although the proposed method does not use the TV norm for removing the twin image in this experiment, it still reconstructs a clearer image with a sparser edge matrix compared to the CS method.

1) PHASE AND AMPLITUDE RECONSTRUCTION

Fig. 5 compares the amplitude reconstruction of the proposed method with the CS method on the simulated USAF resolution chart. The origin image is resized into 1000×1000 pixels before simulation. The illumination light with wavelength $\lambda = 532\mu\text{m}$ and a complementary metal-oxide-semiconductor (CMOS) sensor with a pixel size of $4\mu\text{m}$ is considered when simulating the hologram. The distance between the object plane and the sensor plane is set to 1.2cm . The proposed method reconstructs the image amplitude from the simulated hologram by solving the inverse problem. The quality of the reconstructed image amplitude is higher (i.e. more similar to the ground truth) than the reconstructed image by the the CS algorithm in [17]. Also, a Canny edge detector is used to extract the edge matrix for the enlarged area in these two reconstruction results and the ground truth image [52], [53]. The edge matrix shows that the proposed method has a better denoising capability than the CS method, even without any hand-crafted regularization such as the TV norm.

Further experiments demonstrate that the proposed method dramatically improves upon restoring detailed textures and phase information. The amplitude and phase recovery of a cell image from its simulated hologram is presented in Fig. 6. Apparently, the proposed algorithm outperforms the CS method in restoring finer resolutions and sharper details of the amplitude and creating more precise phase information. This improvement is due to the natural superiority of CNNs for image recovery applications. When simulating the hologram with an explicit phase, we apply the grayscale version of the original RGB image as the reference amplitude and the green channel as the reference phase. The hologram size is 500×500 that are generated with the same light wavelength and the object-to-sensor distance used for the USAF hologram in figure 5. The pixel size here is $1.67\mu\text{m}$. The output of the proposed method exhibits maintaining more structural textures with respect to the ground truth amplitude and phase compared to the CS method.

Similar results are presented for human dendrite image under the same configuration in Fig. 7 as another evidence for the efficiency of the proposed algorithm in recovering amplitude and phase information from holographic recordings.

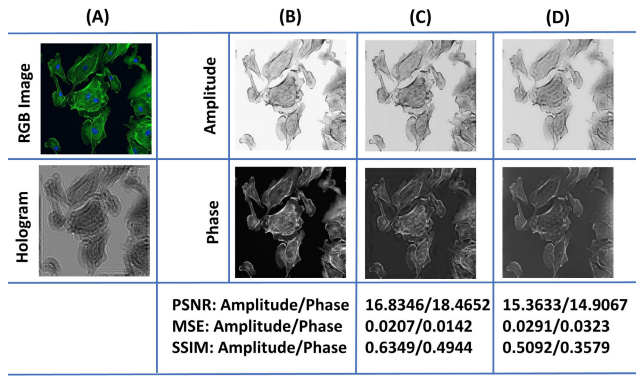


FIGURE 6. Cell image reconstructions from hologram: (A) the RGB image (top) and the simulated hologram (bottom); (B) the reference amplitude and phase; (C) the results of the proposed method; (D) the results of the CS. Our method reconstructs an image with clearer and more detailed texture for both amplitude and phase reflected by a higher SSIM and PSNR compared to the CS algorithm.

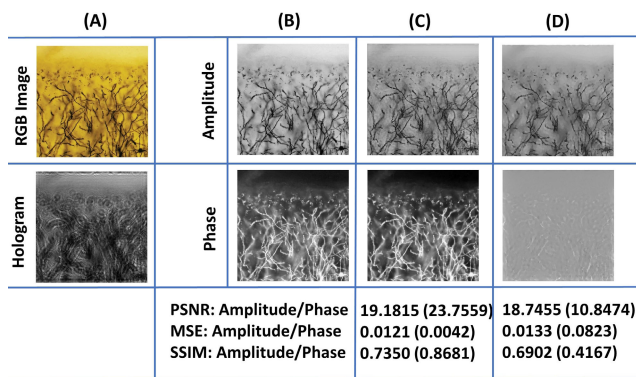


FIGURE 7. Human dendrite image reconstructions along with the performance metrics for the amplitude and phase: (A) the RGB image (top) and the simulated hologram (bottom); (B) the reference amplitude and phase; (C) the results of the proposed method; (D) the results of the CS. In this experiment, the proposed method has shown much better performance in phase information recovery than the CS method. (Figure obtained from [54]).

2) RECONSTRUCTION UNDER NOISE

The captured hologram can be noisy due to environmental factors (dust, low illumination intensity), imperfect sensors, and other imaging artifacts. We investigate the performance of the proposed algorithm when the captured hologram of a “circle” image is contaminated with additive white Gaussian noise. In this experiment, we use different noise levels (variances) at 5, 10, and 15, as shown in Fig.10. Experimental results demonstrate that the proposed method holds a better performance than the CS method when encountering noise in the captured holograms.

3) RECONSTRUCTION WITH DIFFERENT NETWORK INPUT

The input of the neural network, which is used as the initial guess in our reconstruction setup, can dramatically affect the reconstruction quality. We examined the reconstruction with different network inputs, including the captured hologram intensity, the back-propagated hologram by angular spectrum

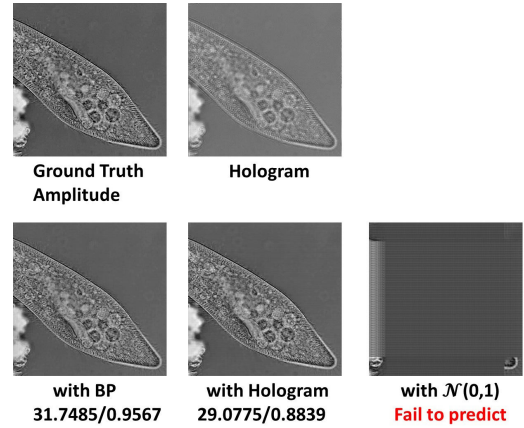


FIGURE 8. Reconstruction on a paramecium hologram. Reconstruction with back-propagated input holds a higher PSNR/SSIM than hologram input while using random Gaussian noise as input failed to converge. (Figure obtained from [55]).

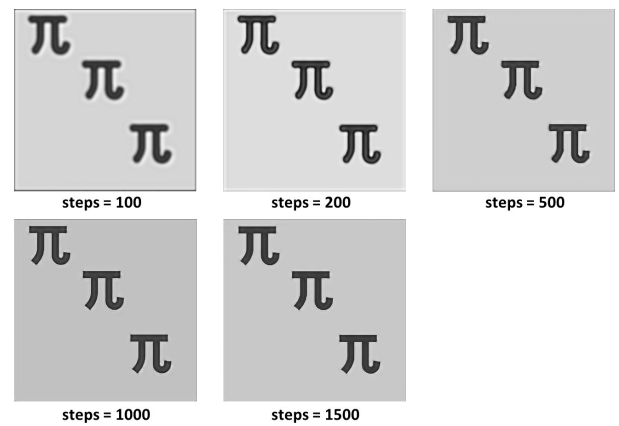


FIGURE 9. Pi image restoration at 100, 200, 500, 1000, and 1500 training steps. Obviously, the rough shape of the object is restored first, then more details and sharp edges are restored.

propagation (ASP), and a random Gaussian noise $N(0, 1)$. Fig.8 shows the reconstruction results of a paramecium hologram with these three network inputs. The best result is obtained when the back-propagated hologram is used as the initial guess, as was expected. If the captured hologram is fed to the network as the initial guess, a reasonable reconstruction can be achieved. However, the output for a random Gaussian noise $N(0, 1)$ is not acceptable, and the network could not converge to the desired point and failed to produce a reasonable result.

4) RECONSTRUCTION ITERATIONS

An experiment on a simulated Pi-shaped image is conducted to examine the convergence of the proposed algorithm. The reconstruction results at different training iterations are shown in Fig. 9. During the optimization process, the CNN first tends to restore the general shape of objects and then gradually adds fine-resolution details to it. This justifies the use of the proposed architecture for phase retrieval. Compared with the object field, the twin image usually exhibit a

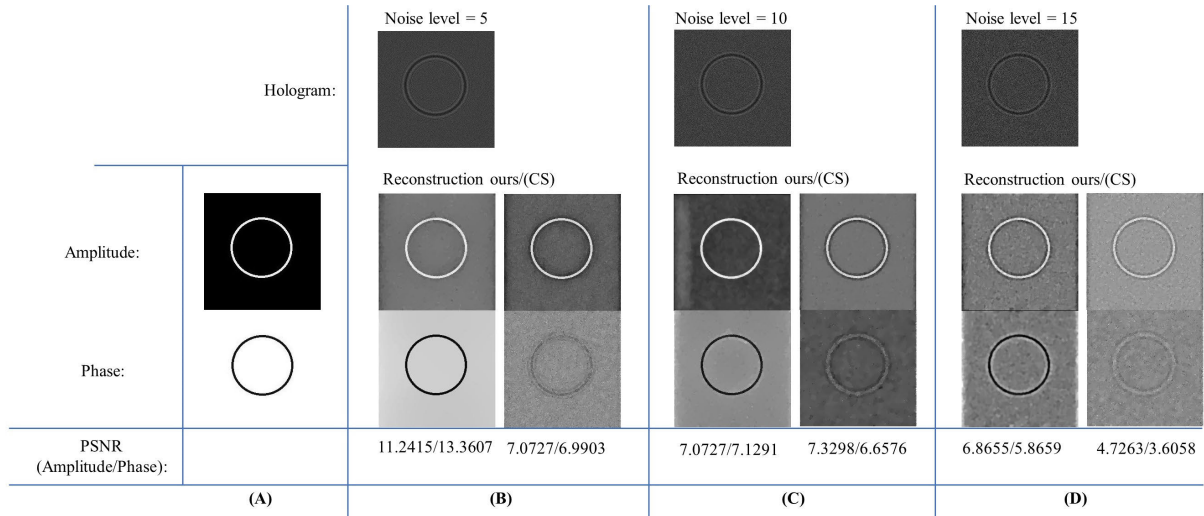


FIGURE 10. Reconstruction under AWGN: (A) the ground truth phase and amplitude. (B) Reconstruction under noise level at 5. (C) Reconstruction under noise level at 10. (D) Reconstruction under noise level at 15.

more obscure pattern. Therefore, when the network is used to restore the object from the captured hologram, it converges to the object field (the actual image) before the twin image is recovered, since clean object field is the solution to the inverse problem.

B. OPTICAL EXPERIMENTS

To verify the performance of the proposed method in real-world situations, a series of optical experiments are conducted using the holograms taken in Dr. Mann’s research laboratory. Fig. 11 illustrates the configuration for the lensless Gabor DHM system used in our experiments. The light source consists of a Thorlabs single-mode fiber-coupled laser. A pig-tailed light beam is emitted to a single-mode fiber that is terminated at an FC/PC bulkhead. The sample is placed between the light source and an image sensor (Imaging Source DMM 27UJ003-ML - pixel size $1.67\mu m$) with an object reconstruction distance z . Performing hologram reconstruction in piratical is a relatively more laborious task than in simulation due to the error between the actual parameters and the preset parameters in the experiment. Meanwhile, the influence of ambient light and air dust in the environment leads to high noise in the real hologram. Therefore, the algorithm applied in real-world data is expected to be robust to noise and optical parameter errors.

Fig. 12 shows the reconstruction result on a USAF positive high-resolution test target (which means the stripes and digits are thicker than the background). An illuminated plane wave at the wavelength of $406\mu m$ is used, and the distance between the target and the image sensor is set at around $z = 1110\mu m$. A multi-height TIE based algorithm is used for comparison with ten captured holograms with a step-size $15\mu m$ between the adjacent hologram planes. In the former deep learning based work [38]–[40], the multi-height TIE based algorithm is used for producing the ground truth of the training pairs

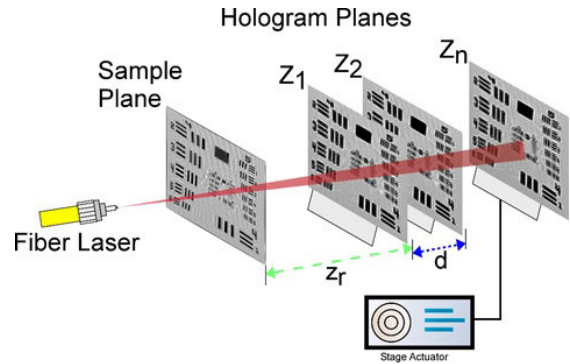


FIGURE 11. The configuration for the lensless digital Gabor holography system.

that have been proven to hold an excellent performance. The reconstructed amplitude and phase show the outstanding denoising and twin image removal capabilities of the proposed method. The reconstructed results have comparable quality to the multi-height methods with single-shot hologram. The enlarged area proves that our approach can retain high-quality details to a great extent while removing the twin image at the same time. The effeteness of the twin image removal ability is quantified as a mean edge factor, which is calculated as $\frac{1}{NM} \sum_{i,j=0}^{N,M} A_{i,j}$, where the $A_{i,j}$ is the edge matrix obtained by the Canny edge detector [52], [53]. We choose the Canny edge detector for getting edge matrix since it is more sensitive than the Sobel operator. The mean edge factors are 0.0990 and 0.1210 respectively for the multi-height method and our deep learning based methodology.

We also show the reconstruction of our method at different training iterations in Fig. 13 to examine the theoretical explanation we proposed in Section. III-A. The results show that our interpretation of why the presented method works still hold true for real-world data.

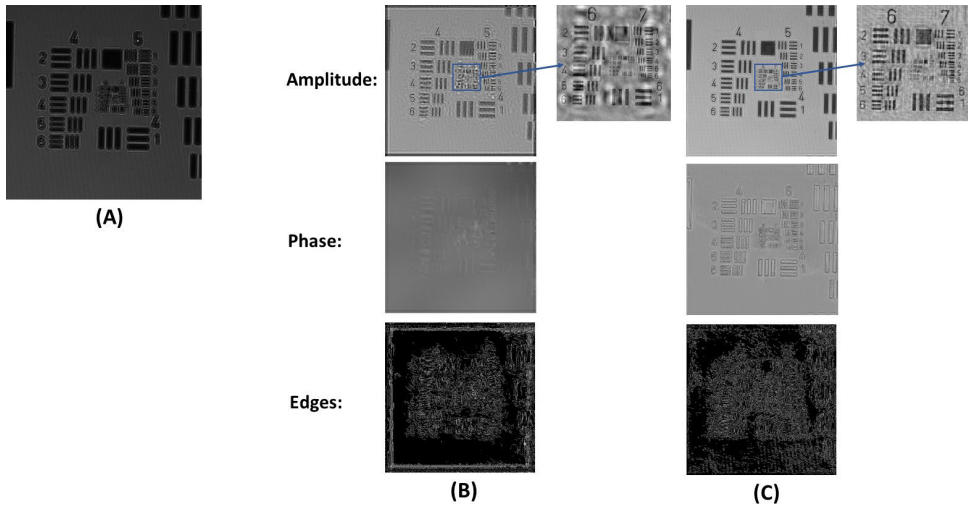


FIGURE 12. (A) The captured hologram of the USAF positive high-resolution test target. (B) Multi-height reconstruction. (C) The proposed deep learning reconstruction.

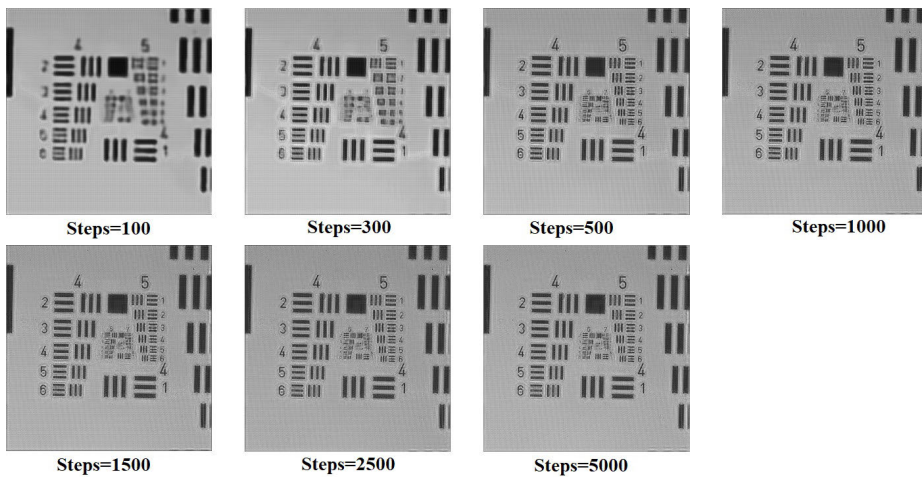


FIGURE 13. USAF positive high-resolution test target restoration at 100, 300, 500, 1000, 1500, 2500, and 500 training epochs. The reconstruction still follows the regular pattern that the rough shape is restored first, and details are restored later.

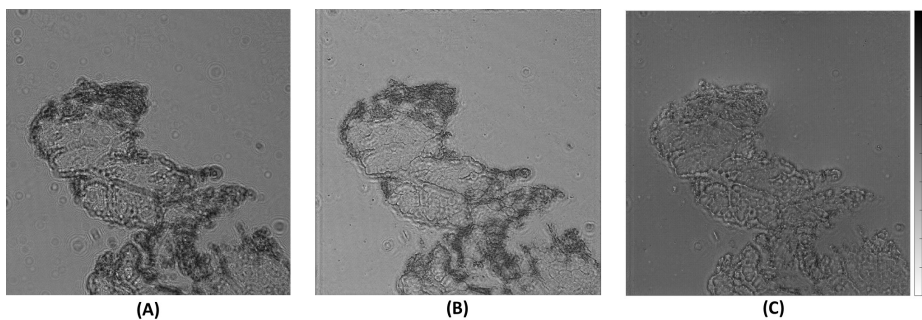


FIGURE 14. Optical Experimental hologram of USAF Resolution Chart and reconstructions. (A) The captured hologram. (B) Amplitude reconstruction with our method. (C) The reconstructed quantitative phase with our method.

An experiment on a sectioned dysplasia tonsillar mucosa tissue is conducted to verify the potential of our method on biomedical usage. The tissue holography could be used to analyze beforehand with clinical histological diagnosis.

The hologram is captured with an illuminated plane wave with a wavelength at $0.635 \mu\text{m}$ and an object to sensor distance set at $857 \mu\text{m}$. Fig. 14 shows the captured hologram and reconstruction. The reconstructed phase shows the tissue

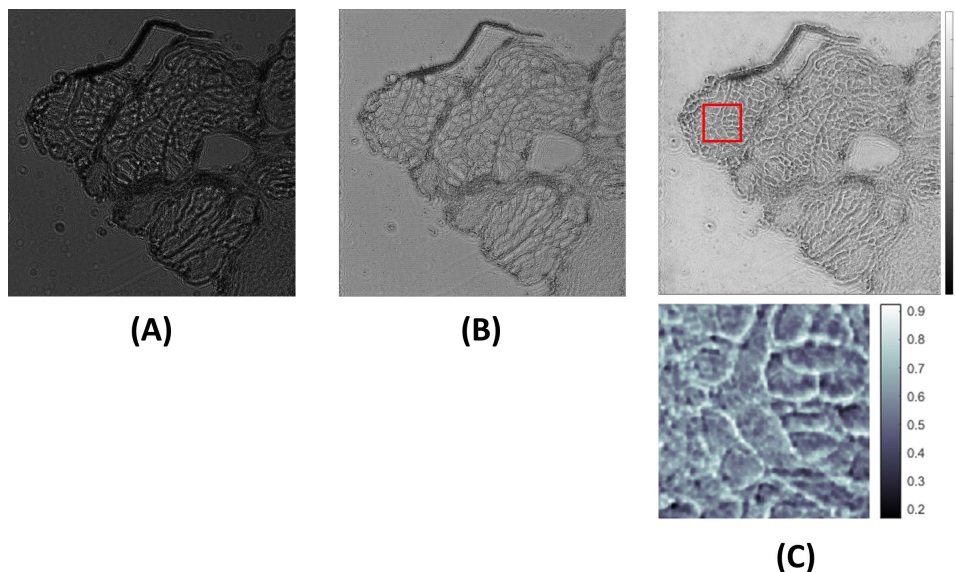


FIGURE 15. Optical Experimental hologram of a non-keratinizing squamous cell carcinoma and reconstructions. (A) The captured hologram. (B) Amplitude reconstruction with our method. (C) The reconstructed quantitative phase with our approach.

structure's relative depth that could be used to reconstruct the 3D surface of the tissue. Another experiment on a non-keratinizing squamous cell carcinoma is shown in Fig.15 also proves the effectiveness of the proposed method on biomedical imaging.

V. CONCLUSION

A deep learning method for single-shot reconstruction of in-line digital holography reconstruction is proposed in this article. The key advantage of the proposed method compared to similar numerical Reconstruction methods and the recently developed DL-based methods is two-fold. Firstly, the proposed method achieves a considerably improved performance using single-shot imaging and eliminates the need for multiple imaging. Secondly, no training dataset is required to train the utilized neural network compared to similar DL-based methods. The physical symmetry of the holography equations implies that the object image and the twin image both can be the solution of the resulting inverse problem. With a given prior, the proposed Auto-encoder architecture is able to reconstruct the object image. The proposed method has been proven powerful and potential through both simulated and optical hologram experiments. Although most of the DL-based methods are relatively time-consuming compared to the complex experimental setup of multi-height phase retrieval, our method is cost-effective and computationally affordable.

REFERENCES

- [1] F. Matsui, K. Yasuda, N. Maejima, H. Matsui, T. Matsushita, and H. Daimon, "Chemical and magnetic properties of polycrystalline iron surface revealed by auger electron holography, spectroscopy, and microscopy," *Jpn. J. Appl. Phys.*, vol. 58, no. 11, Nov. 2019, Art. no. 110602.
- [2] W. Xu, M. Jericho, I. Meinertzhagen, and H. Kreuzer, "Digital in-line holography for biological applications," *Proc. Nat. Acad. Sci. USA*, vol. 98, no. 20, pp. 11301–11305, 2001.
- [3] G. Zheng, H. Mühlenbernd, M. Kenney, G. Li, T. Zentgraf, and S. Zhang, "Metasurface holograms reaching 80% efficiency," *Nature Nanotechnol.*, vol. 10, no. 4, pp. 308–312, Apr. 2015.
- [4] P. S. Ramanujam, "Optical fabrication of nano-structured biopolymer surfaces," *Opt. Mater.*, vol. 27, no. 6, pp. 1175–1177, Mar. 2005.
- [5] R. L. van Renesse, "Synergistic combination of document security techniques," *Proc. SPIE*, vol. 3973, pp. 126–138, Apr. 2000.
- [6] E. Cuche, P. Marquet, and C. Depeursinge, "Simultaneous amplitude-contrast and quantitative phase-contrast microscopy by numerical reconstruction of Fresnel off-axis holograms," *Appl. Opt.*, vol. 38, no. 34, pp. 6994–7001, Dec. 1999.
- [7] E. N. Leith and J. Upatnieks, "Wavefront reconstruction with continuous-tone objects," *JOSA*, vol. 53, no. 12, pp. 1377–1381, 1963.
- [8] G. Gabor, "A new microscopic principle," *Nature*, vol. 161, pp. 177–178, May 1948. [Online]. Available: <https://www.nature.com/articles/Art56>, doi: 10.1038/161777a0.
- [9] T. Latychevskaia and H.-W. Fink, "Solution to the twin image problem in holography," *Phys. Rev. Lett.*, vol. 98, no. 23, Jun. 2007, Art. no. 233901.
- [10] M. Beleggia, M. A. Schofield, V. V. Volkov, and Y. Zhu, "On the transport of intensity technique for phase retrieval," *Ultramicroscopy*, vol. 102, no. 1, pp. 37–49, Dec. 2004.
- [11] L. Denis, C. Fournier, T. Fournel, and C. Ducottet, "Twin-image noise reduction by phase retrieval in in-line digital holography," *Proc. SPIE*, vol. 5914, Sep. 2005, Art. no. 59140J.
- [12] G. Liu and P. D. Scott, "Phase retrieval and twin-image elimination for in-line fresnel holograms," *JOSA A*, vol. 4, no. 1, pp. 159–165, 1987.
- [13] J. R. Fienup, "Phase retrieval algorithms: A comparison," *Appl. Opt.*, vol. 21, no. 15, pp. 2758–2769, Aug. 1982.
- [14] R. W. Gerchberg, "A practical algorithm for the determination of phase from image and diffraction plane pictures," *Optik*, vol. 35, no. 2, pp. 237–246, 1972.
- [15] S. Flewett, C. Günther, C. V. K. Schmising, B. Pfau, J. Mohanty, F. Büttner, M. Riemeier, M. Hantschmann, M. Kläui, and S. Eisebitt, "Holographically aided iterative phase retrieval," *Opt. Express*, vol. 20, no. 28, pp. 29210–29216, 2012.
- [16] W.-J. Zhou, X. Guan, F. Liu, Y. Yu, H. Zhang, T.-C. Poon, and P. P. Banerjee, "Phase retrieval based on transport of intensity and digital holography," *Appl. Opt.*, vol. 57, no. 1, pp. A229–A234, 2018.

- [17] W. Zhang, L. Cao, D. J. Brady, H. Zhang, J. Cang, H. Zhang, and G. Jin, "Twin-Image-Free holography: A compressive sensing approach," *Phys. Rev. Lett.*, vol. 121, no. 9, Aug. 2018, Art. no. 093902.
- [18] L. J. Allen and M. P. Oxley, "Phase retrieval from series of images obtained by defocus variation," *Opt. Commun.*, vol. 199, nos. 1–4, pp. 65–75, Nov. 2001.
- [19] L. Waller, L. Tian, and G. Barbastathis, "Transport of intensity phase-amplitude imaging with higher order intensity derivatives," *Opt. Express*, vol. 18, no. 12, p. 12 552–12 561, 2010.
- [20] S. Tong, H. Li, and H. Huang, "Energy extension in three-dimensional atomic imaging by electron emission holography," *Phys. Rev. Lett.*, vol. 67, no. 22, p. 3102, 1991.
- [21] J. Barton, "Removing multiple scattering and twin images from holographic images," *Phys. Rev. Lett.*, vol. 67, no. 22, p. 3106, 1991.
- [22] M. R. Teague, "Deterministic phase retrieval: A Green's function solution," *JOSA*, vol. 73, no. 11, pp. 1434–1441, 1983.
- [23] T. Gureyev, A. Roberts, and K. Nugent, "Partially coherent fields, the transport-of-intensity equation, and phase uniqueness," *JOSA A*, vol. 12, no. 9, pp. 1942–1946, 1995.
- [24] C. Zuo, Q. Chen, W. Qu, and A. Asundi, "Direct continuous phase demodulation in digital holography with use of the transport-of-intensity equation," *Opt. Commun.*, vol. 309, pp. 221–226, Nov. 2013.
- [25] L. Waller, Y. Luo, S. Y. Yang, and G. Barbastathis, "Transport of intensity phase imaging in a vol. holographic microscope," *Opt. Lett.*, vol. 35, no. 17, pp. 2961–2963, 2010.
- [26] M. Krenkel, M. Bartels, and T. Salditt, "Transport of intensity phase reconstruction to solve the twin image problem in holographic X-ray imaging," *Opt. Express*, vol. 21, no. 2, pp. 2220–2235, 2013.
- [27] M. Soto and E. Acosta, "Improved phase imaging from intensity measurements in multiple planes," *Appl. Opt.*, vol. 46, no. 33, pp. 7978–7981, 2007.
- [28] T. E. Gureyev, "Composite techniques for phase retrieval in the fresnel region," *Opt. Commun.*, vol. 220, nos. 1–3, pp. 49–58, May 2003.
- [29] T. E. Gureyev, Y. I. Nesterets, D. M. Paganin, A. Pogany, and S. W. Wilkins, "Linear algorithms for phase retrieval in the fresnel region. 2. Partially coherent illumination," *Opt. Commun.*, vol. 259, no. 2, pp. 569–580, Mar. 2006.
- [30] M. Guizar-Sicairos and J. R. Fienup, "Understanding the twin-image problem in phase retrieval," *JOSA A*, vol. 29, no. 11, pp. 2367–2375, 2012.
- [31] Z. Zalevsky, D. Mendlovic, and R. G. Dorsch, "Gerchberg–Saxton algorithm applied in the fractional Fourier or the Fresnel domain," *Opt. Lett.*, vol. 21, no. 12, pp. 842–844, Jun. 1996.
- [32] H. H. Bauschke, P. L. Combettes, and D. R. Luke, "Phase retrieval, error reduction algorithm, and fienuip variants: A view from convex optimization," *J. Opt. Soc. Amer. A, Opt. Image Sci.*, vol. 19, no. 7, pp. 1334–1345, 2002.
- [33] J. R. Fienup, "Reconstruction of an object from the modulus of its Fourier transform," *Opt. Lett.*, vol. 3, no. 1, pp. 27–29, Jul. 1978.
- [34] S. Wang, H. Cheng, L. Ying, T. Xiao, Z. Ke, H. Zheng, and D. Liang, "DeepcomplexMRI: Exploiting deep residual network for fast parallel MR imaging with complex convolution," *Magn. Reson. Imag.*, vol. 68, pp. 136–147, May 2020.
- [35] C. M. Hyun, H. P. Kim, S. M. Lee, S. Lee, and J. K. Seo, "Deep learning for undersampled MRI reconstruction," *Phys. Med. Biol.*, vol. 63, no. 13, Jun. 2018, Art. no. 135007.
- [36] G. Yang, S. Yu, H. Dong, G. Slabaugh, P. L. Dragotti, X. Ye, F. Liu, S. Arridge, J. Keegan, Y. Guo, and D. Firmin, "DAGAN: Deep de-aliasing generative adversarial networks for fast compressed sensing MRI reconstruction," *IEEE Trans. Med. Imag.*, vol. 37, no. 6, pp. 1310–1321, Jun. 2018.
- [37] S. Wang, Z. Su, L. Ying, X. Peng, S. Zhu, F. Liang, D. Feng, and D. Liang, "Accelerating magnetic resonance imaging via deep learning," in *Proc. IEEE 13th Int. Symp. Biomed. Imag. (ISBI)*, Apr. 2016, pp. 514–517.
- [38] R. Horisaki, R. Takagi, and J. Tanida, "Deep-learning-generated holography," *Appl. Opt.*, vol. 57, no. 14, pp. 3859–3863, 2018.
- [39] Y. Rivenson, Y. Zhang, H. Günaydin, D. Teng, and A. Ozcan, "Phase recovery and holographic image reconstruction using deep learning in neural networks," *Light, Sci. Appl.*, vol. 7, no. 2, p. 17141, 2018.
- [40] W.-C. Gan and F.-W. Shu, "Holography as deep learning," *Int. J. Mod. Phys. D*, vol. 26, no. 12, 2017, Art. no. 1743020.
- [41] P. Langehanenber, B. Kemper, D. Dirksen, and G. von Bally, "Autofocusing in digital holographic phase contrast microscopy on pure phase objects for live cell imaging," *Appl. Opt.*, vol. 47, no. 19, pp. D176–D182, 2008.
- [42] L. Rong, Y. Li, S. Liu, W. Xiao, F. Pan, and D. Wang, "Iterative solution to twin image problem in in-line digital holography," *Opt. Lasers Eng.*, vol. 51, no. 5, pp. 553–559, May 2013.
- [43] C. Cho, B. Choi, H. Kang, and S. Lee, "Numerical twin image suppression by nonlinear segmentation mask in digital holography," *Opt. Express*, vol. 20, no. 20, pp. 22454–22464, 2012.
- [44] V. Lempitsky, A. Vedaldi, and D. Ulyanov, "Deep image prior," in *Proc. IEEE/CVF Conf. Comput. Vis. Pattern Recognit.*, Jun. 2018, pp. 9446–9454.
- [45] S. Ioffe and C. Szegedy, "Batch normalization: Accelerating deep network training by reducing internal covariate shift," 2015, *arXiv:1502.03167*. [Online]. Available: <http://arxiv.org/abs/1502.03167>
- [46] V. Nair and G. E. Hinton, "Rectified linear units improve restricted Boltzmann machines," in *Proc. ICML*, 2010, pp. 1–8.
- [47] Y. Rivenson, Y. Wu, H. Wang, Y. Zhang, A. Feizi, and A. Ozcan, "Sparsity-based multi-height phase recovery in holographic microscopy," *Sci. Rep.*, vol. 6, no. 1, p. 37862, Dec. 2016.
- [48] O. Ronneberger, P. Fischer, and T. Brox, "U-Net: Convolutional networks for biomedical image segmentation," in *Medical Image Computing and Computer-Assisted Intervention (MICCAI)*. Munich, Germany: Springer, Oct. 2015, pp. 234–241. [Online]. Available: <https://www.springer.com/gp/book/9783319245522>
- [49] A. Paszke, S. Gross, F. Massa, A. Lerer, J. Bradbury, G. Chanan, T. Killeen, Z. Lin, N. Gimelshein, L. Antiga, and A. Desmaison, "Pytorch: An imperative style, high-performance deep learning library," in *Proc. Adv. Neural Inf. Process. Syst.*, 2019, pp. 8024–8035.
- [50] D. P. Kingma and J. Ba, "Adam: A method for stochastic optimization," 2014, *arXiv:1412.6980*. [Online]. Available: <http://arxiv.org/abs/1412.6980>
- [51] Z. Wang, A. C. Bovik, H. R. Sheikh, and E. P. Simoncelli, "Image quality assessment: From error visibility to structural similarity," *IEEE Trans. Image Process.*, vol. 13, no. 4, pp. 600–612, Apr. 2004.
- [52] W. McIlhagga, "The canny edge detector revisited," *Int. J. Comput. Vis.*, vol. 91, no. 3, pp. 251–261, Feb. 2011.
- [53] L. Ding and A. Goshtasby, "On the Canny edge detector," *Pattern Recognit.*, vol. 34, no. 3, pp. 721–725, Mar. 2001.
- [54] P. Stern. (Jan. 2020). *Human Dendrites are Special*. [Online]. Available: <https://science.sciencemag.org/content/367/6473/36.1>
- [55] *Live Paramecium 100X*. Accessed: Mar. 10, 2020. [Online]. Available: <https://www.luc.edu/biology/111lab/5-theprotists/photos/paramecium-3/>



HUAYU LI received the B.S. degree in computer engineering from Northern Arizona University, USA, in 2019, where he is currently pursuing the degree in electrical engineering. His research interests include low-level problem in computer vision, digital holography, and deep learning, supervised by Dr. Razi.



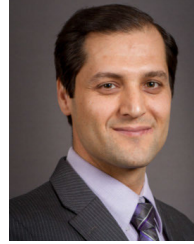
XIWEN CHEN (Student Member, IEEE) received the B.S. degree in electrical engineering from Northern Arizona University, in 2019, where he is currently pursuing the Ph.D. degree in informatics and cyber systems. His current research interests include developing image-based security protocols, and information retrieval in complex networks.



ZAOYI CHI received the B.S. degree in electrical engineering from the Chongqing University of Posts and Telecommunications, China, in 2018. He is currently pursuing the degree in electrical engineering with Northern Arizona University. His research interests include machine learning, computer vision, the IoT security, and deep learning, supervised by Dr. Abolfazl Razi.



CHRISTOPHER MANN is currently an Associate Professor with the Department of Applied Physics and Materials Science, NAU. His research interests include image design and acquisition, reconstruction, processing, and analysis. More specifically, his focus is on developing new methods for non-destructive testing and analysis, image processing, and image-based metrology using holography and interferometry. He has extensive experience in the use of optical design software, such as Zemax, optical design, and prototyping. He is proficient in the use of a number of programming languages. His research expertise is primarily centered on the field of optics, and in particular optical interferometry and holography. His current research program conducts applied optics research and development addressing important issues of industrial and economic competitiveness, biomedical measurement science, and national security. He was awarded the Eugene P. Wigner Postdoctoral Fellowship at the Oak Ridge National Laboratory to develop work in optical interferometry, through which he made contributions in a number of application areas, including industrial inspection, biological microscopy, as well as MEMS characterization for which he has three patents awarded.



ABOLFAZL RAZI (Senior Member, IEEE) received the B.S. degree from Sharif University, in 1998, the M.S. degree from Tehran Polytechnic, in 2001, and the Ph.D. degree from the University of Maine, in 2013, all in electrical engineering. He is currently an Assistant Professor with the School of Informatics, Computing, and Cyber Systems, Northern Arizona University (NAU). Prior to joining NAU, he held two postdoctoral positions in the field of machine learning and predictive modeling at Duke University, from 2013 to 2014, and Case Western Reserve University, from 2014 to 2015. His current research interests include smart connected communities, biomedical signal processing, wireless networking, the Internet of Things, and predictive modeling. He was a recipient of several competitive awards, including the Best Research of MCI in 2008, the Best Graduate Research Assistant of the Year Award from the College of Engineering, University of Maine, in 2011, and the Best Paper Award from the IEEE/CANEUS Fly by Wireless Workshop, in 2011.

...